

# Palynological evidence for the astronomical origin of lignite–detritus sequence in the Middle Pleistocene Marathousa Member, Megalopolis, SW Greece

M. Okuda<sup>a,\*</sup>, N. van Vugt<sup>b</sup>, T. Nakagawa<sup>c</sup>, M. Ikeya<sup>d</sup>, A. Hayashida<sup>e</sup>,  
Y. Yasuda<sup>c</sup>, T. Setoguchi<sup>f</sup>

<sup>a</sup> Natural History Museum and Institute, Chiba, 955-2 Aoba, Chiba 260-8682, Japan

<sup>b</sup> Paleomagnetic Laboratory 'Fort Hoofddijk', Faculty of Earth Sciences, Utrecht University, Budapestlaan 14, 3584 CD Utrecht, The Netherlands

<sup>c</sup> International Research Centre for Japanese Studies, Kyoto 610-1192, Japan

<sup>d</sup> Department of Earth and Space Science, Graduate School of Science, Osaka University, Osaka 560-0043, Japan

<sup>e</sup> Science and Engineering Institute, Doshisha University, Kyo-tanabe 610-0321, Japan

<sup>f</sup> Department of Geology and Mineralogy, Division of Earth and Planetary Sciences, Kyoto University, Kyoto 606-8224, Japan

Received 7 January 2002; received in revised form 14 April 2002; accepted 29 April 2002

## Abstract

The Marathousa Member, Middle Pleistocene strata in the fluvio-lacustrine Megalopolis basin, southwest Greece, displays distinct but complicated lithological cycles comprising first-order alternation of lignites and detrital muds and second-order alternation expressed by frequent intercalation of organic layers. Palynological evidence indicates that the lithological cycles are driven by the Earth's orbital forcing. All the lignite seams yield temperate oak forest whereas the detrital beds provide semi-arid steppe mainly of *Artemisia*. This means that the first-order lithological cycle represents the glacial/interglacial cycle (i.e., the 100-kyr eccentricity cycle), providing a timescale of at least 350 kyr to the Marathousa Member. Pollen also detects smaller-scale climate fluctuations in many of the subordinate organic layers, with the total number of fluctuations being five in a complete lignite–detritus couplet. This means that the second-order lithological cycle reflects the 21-kyr insolation cycle. A tentative phase relation between the lithological cycles and the astronomical cycles is shown based on palynostratigraphy and electron spin resonance dating. Lacustrine environments with increased water tables are implied for the glacial periods sedimentologically, in contrast to local swamp vegetation for the interglacial periods. The subordinate organic layers were formed under intermediate environments (climate, water depth, etc.) between full glacial and interglacial. © 2002 Elsevier Science B.V. All rights reserved.

**Keywords:** orbital forcing; Middle Pleistocene; Greece; palynology; EPR spectra; age; climate change

## 1. Introduction

In the Mediterranean region, distinct lithological cycles occur in sedimentary basins from differ-

\* Corresponding author. Fax: +81-43-266-2481.

E-mail address: okuda@chiba-muse.or.jp (M. Okuda).

ent periods and environments. These lithological cycles consist of a dozen couplets of marl, detritus (silt/clay) or organic beds (lignite/sapropel), showing rhythmic alternation in ca. 100-m composite sections [1–5]. Understanding the origins and formation processes of these lithological cycles can lead to the acquisition of remarkably age-secured geological archives with cyclic paleoclimate and paleoenvironmental records.

It has been accepted that long-term climate changes are controlled by variation in the parameters of the Earth's orbit [6,7]. For marine deposits beneath the Mediterranean Sea, a linkage between sedimentary cycles and astronomical cycles has been indicated [8–10]. Correlations are anchored by frequent paleomagnetic polarity reversals as well as marine biostratigraphy based on planktonic foraminifera and calcareous nannoplankton. Good agreements between the calibrated duration of a lithological cycle and the computed duration of an astronomical cycle secure the linkage. This has led to the establishment of the astronomical polarity time scale (APTS) [11,12], which provides standard astronomical ages for major geomagnetic events of the Neogene to the Quaternary.

Recently, the above cyclostratigraphic techniques have also been applied to continental deposits without reference to marine biostratigraphy [13–16]. In many cases, small continental basins have higher sedimentation rates than large oceanic basins. Hilgen et al. [17] have stressed the advantage of continental basins as logical places to detect Milankovitch cycles more directly, because of their isolation from oceanographic processes with intrinsic non-linear mechanisms. Most of the above case studies for continental basins, however, have been restricted to the Neogene with detailed APTS [18] and unprecedented marine reference sections [3]. In the Pliocene lacustrine Ptolemais basin of northern Greece, rhythmic alternation of white/beige marl and blackish lignite has been anchored by four paleomagnetic subchrons (Thvera, Sidufjall, Nunivak and Cochiti), attributed to the 21-kyr insolation cycle on the basis of correlations with astronomical target curves [19]. Lignite seams were attributed to insolation minima (cold stages) with lowered lake

levels, while marl beds were assigned to insolation maxima (warm stages) with increased precipitation and probably high lake levels.

Unfortunately, unambiguous correlations with the orbital parameters are more difficult for Pleistocene continental deposits. Since 1 Ma, in particular, geomagnetic polarity reversals have been less frequent, and the 100-kyr glacial cycle has become dominant together with other persistent Milankovitch cycles [6,7]. This can give a complex of lithological cycles with different orders to late Pleistocene sediments. The Megalopolis basin is one example of (Plio-)Pleistocene continental basins in the Mediterranean region. The Marathousa Member, which comprises Middle Pleistocene lacustrine deposits in the Megalopolis basin, displays distinct but complicated lithological cycles consisting of blackish lignite, dark gray silty clay and light gray fine-grained detritus. Unlike the Ptolemais basin [19], the lignite seams at Megalopolis cannot be attributed to glacial periods because of the previous palynological work [20] reporting temperate oak forest from the lowermost lignite seam (Lignite I), suggesting a warm stage (interglacial/interstadial). However, limited information on paleoclimate has hindered understanding of the origins and formation processes of the lithological cycles.

This paper presents detailed palynological results to provide the paleoenvironmental background to the Marathousa Member. A loss-on-ignition analysis was performed to quantify the lithological changes. Electron spin resonance (ESR) dating was carried out to yield a new age control point for the Marathousa Member.

## 2. Geology, chronostratigraphy, modern climate and vegetation

The Megalopolis Basin is an intermontane basin located near the center of the Peloponnesos Peninsula, SW Greece (37°25'N, 22°10'E, 400 m a.s.l.) [21] (Fig. 1). The eastern margin of the basin consists of normal faults extending from NW to SE, leading to active tectonic subsidence and deposition during the Pliocene and the Pleistocene. The stratigraphic framework of the Mega-

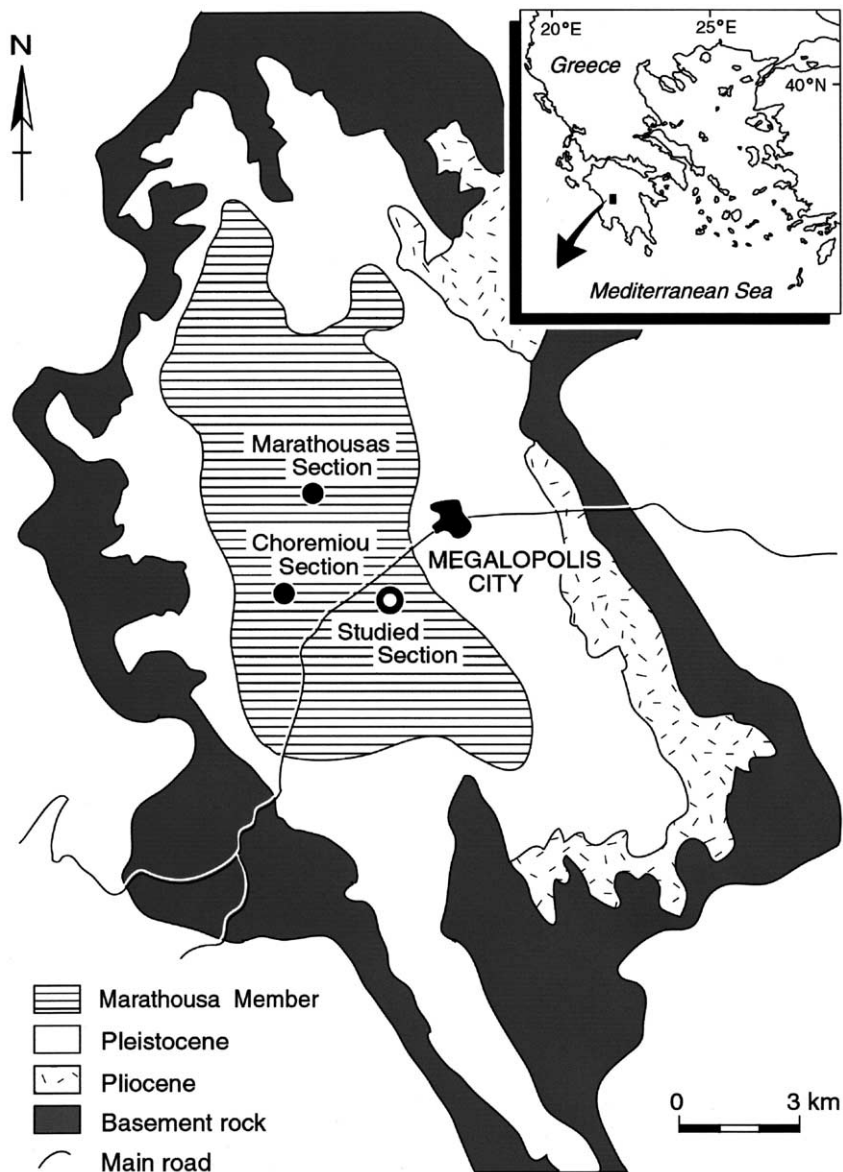


Fig. 1. Geological map of the Megalopolis basin, SW Greece (after [21]). Localities of the studied section as well as parallel Marathousas and Choremiou sections [16] are shown. At present, the Holocene and part of the Pleistocene deposits have been scraped off due to opencast coal mining.

lopolis basin was established by Vinken [22]. The Plio–Pleistocene, which overlies the Paleogene marine basement unconformably, consists of six formations of Makrision, Trilofon, Apidhitsa, Choremi, Potamia and Thoknia from the base upward (Table 1). These represent two large-scale progradation cycles from swamp/lacustrine envi-

ronments in the Makrision and Choremi formations to fluvial/terrestrial environments in the Trilofon/Apidhitsa and Potamia/Thoknia formations. The Marathousa Member forms the lower half of the Choremi Formation. It consists of lacustrine muds yielding freshwater bivalve and ostracod fossils [23], intercalated with lignite seams

Table 1  
Stratigraphy and first-order chronology for the Plio–Pleistocene in the Megalopolis basin, SW Greece (after [22])

Formation	Member	Sediment type	Origin	Climate	Period
(Holocene)		sand, gravel	fluvial, erosion	warm	Holocene
Thoknia		sand, gravel	fluvial	cold	Pleistocene
		brown loam	erosion	warm	Pleistocene
Potamia		sand, gravel	fluvial	cold	Pleistocene
		brown loam	erosion	warm	Pleistocene
Choremi	Megalopolis	sand, gravel	fluvial	cold	Pleistocene
	Marathousa	lignite, clay, silt	lacustrine	warm	Pleistocene
Apidhitsa		sand, gravel	fluvial	cold	Pleistocene
Trilofon		sand, gravel, marl	fluvial	cool	Pliocene
Makrision		lignite, marl	lacustrine	warm	Pliocene

ca. 20 m thick. Three opencast coal mines are present in the Megalopolis basin, providing cross-sections up to 25 m high. The lignites in the Marathousa Member have been studied repeatedly for geological and economical reasons, summarized into five major lignite seams (Lignites I, II, III, IV and V) [16,20].

A first-order timescale for the Marathousa Member was provided by paleontology and magnetostratigraphy. The Marathousa Member does not yield extinct Tertiary-type pollen such as *Taxus*, *Taxodium*, *Sequoia*, *Tsuga*, *Keteleeria* or *Liquidambar*, which characterize the Pliocene Makrision Formation [22]. Cheek teeth of *Mus* cf. *spretus* occurred in Lignite III, giving a Biharian age (middle Pleistocene) to the Marathousa Member [16]. Van Vugt et al. [16] also detected reversed paleomagnetic polarity near the base of the Marathousas and Choremiou sections. Due to a certain paleomagnetically gray zone near the reversal, the Brunhes/Matuyama paleomagnetic boundary was suggested in the upper part of Lignite I or the overlying detrital bed. There was no strong evidence determining the upper limit of the Marathousa Member.

The present climate type of the Megalopolis basin is Mediterranean. Most rain falls in winter, while summers are hot and dry. The Megalopolis basin is located to the west of the mountains near the center of the peninsula, which interrupts the westerly winds and creates a rain shadow in the eastern flank. This geographic property gives relatively high precipitation (750–1000 mm/yr) to the Megalopolis basin. Mean January temperatures

are 7–9°C, resulting in warm, frost-free winters. This is in contrast to the northern Greek inlands where winter frost occurs [24].

The natural vegetation around Megalopolis comprised Mediterranean evergreen woodlands of *Pinus halepensis*, *Quercus ilex* etc., but this vegetation has been completely destroyed by severe tree cutting and sheep grazing. At present, secondary maquis of *Quercus coccifera*, *Pistacia lentiscus*, *Olea* etc. extends to the mountain summits. Small patches of deciduous forest exist in the mid-altitude zones (~700 m), consisting of *Quercus pubescens*, *Fraxinus ornus*, *Carpinus orientalis*, *Ostrya carpinifolia* and *Acer monspessulanum*. At higher altitudes (700–1700 m), *Abies cephalonica* forms montane forests [24].

### 3. Materials and methods

The sampled section is located about 2.5 km to the southwest of Megalopolis city (Fig. 1). In 1994, the section consisted of a series of outcrops with a total height of 70 m, forming the southern margin of one of the opencast mines. Blackish lignite seams ca. 20 m thick alternated with detrital beds of light gray to greenish gray silty clay (Fig. 2). Bedding planes were sharp and flat with no meaningful lateral changes throughout the section.

Nine lithostratigraphic units consisting of four lignite seams alternating with five detrital beds are recognized (units 1–9) (Fig. 3). This first-order lithological cycle is frequently intercalated with

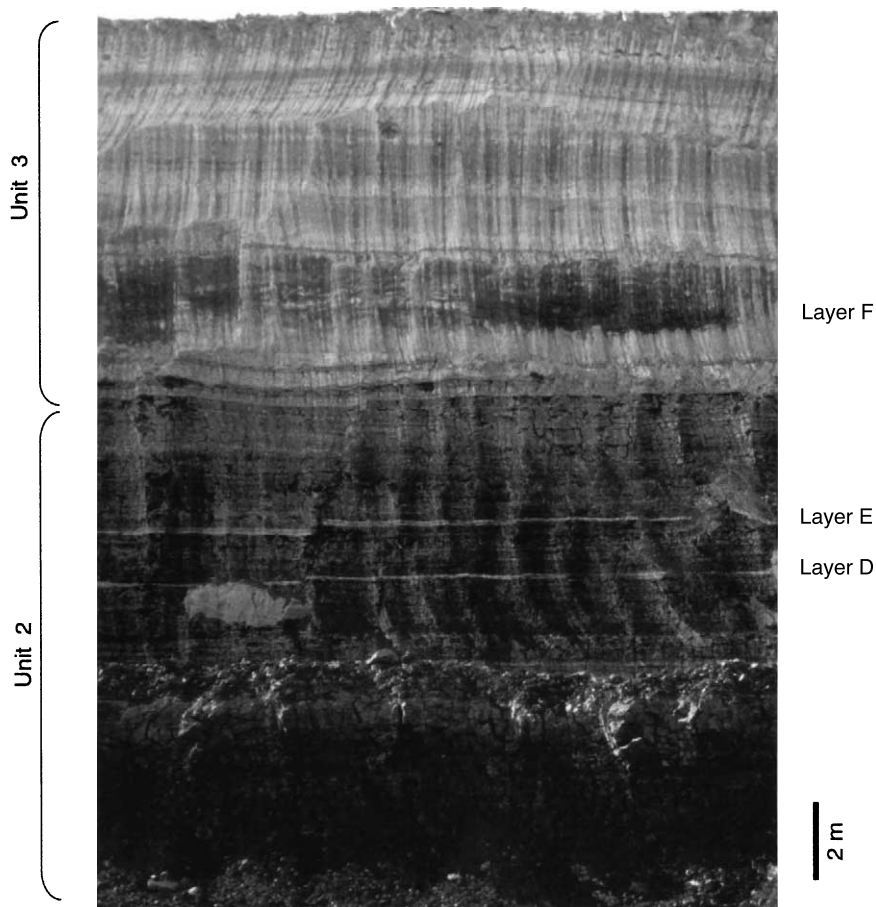


Fig. 2. Photograph of 15–27-m interval of the studied section, Megalopolis, SW Greece.

subordinate dark gray-colored layers. In field observation, this second-order lithological cycle occurs less regularly resisting a comprehensive description. In this paper, 13 major subordinate layers within the units are labelled (layers A–M) with the aim of searching climate signals. The dark gray layers at unit boundaries are not labelled, because these probably reflect glacial/interglacial transitions rather than representing independent climate events. Further information on each lithological unit follows, beginning from the base upward.

Unit 1 (0–5.0 m). Greenish-gray silt/clay. Dark gray layers interbedded near the top of the unit.

Unit 2 (5.0–20.5 m). Blackish lignite with frequent dark gray silt/clay layers of ca. 1 m thickness. Five of the subordinate layers are prominent

and are labelled (layers A–E). A minor band of reddish silt with carbonate fractions occurs at 14 m in the stratigraphic level. The lignite seam contains abundant organic fractions in the lower part, and is slightly laminated in the upper part. The dark gray-colored bed at the top of unit 2 is recognized as a transitional zone between units and is not labelled.

Unit 3 (20.5–33.25 m). Greenish-gray silt/clay. Dark gray silty clay occurs at 22.5–24.5 m, and is labelled F. The sediments contain very fine-grained sands in the upper part of the unit.

Unit 4 (33.25–41.5 m). Blackish lignite with dark gray silt/clay bands. Two subordinate layers are prominent and are labelled G and H. Brownish-gray silt occurs at the top of the unit. At 34 m, small (< 5 mm) gastropod shells are abundant. A

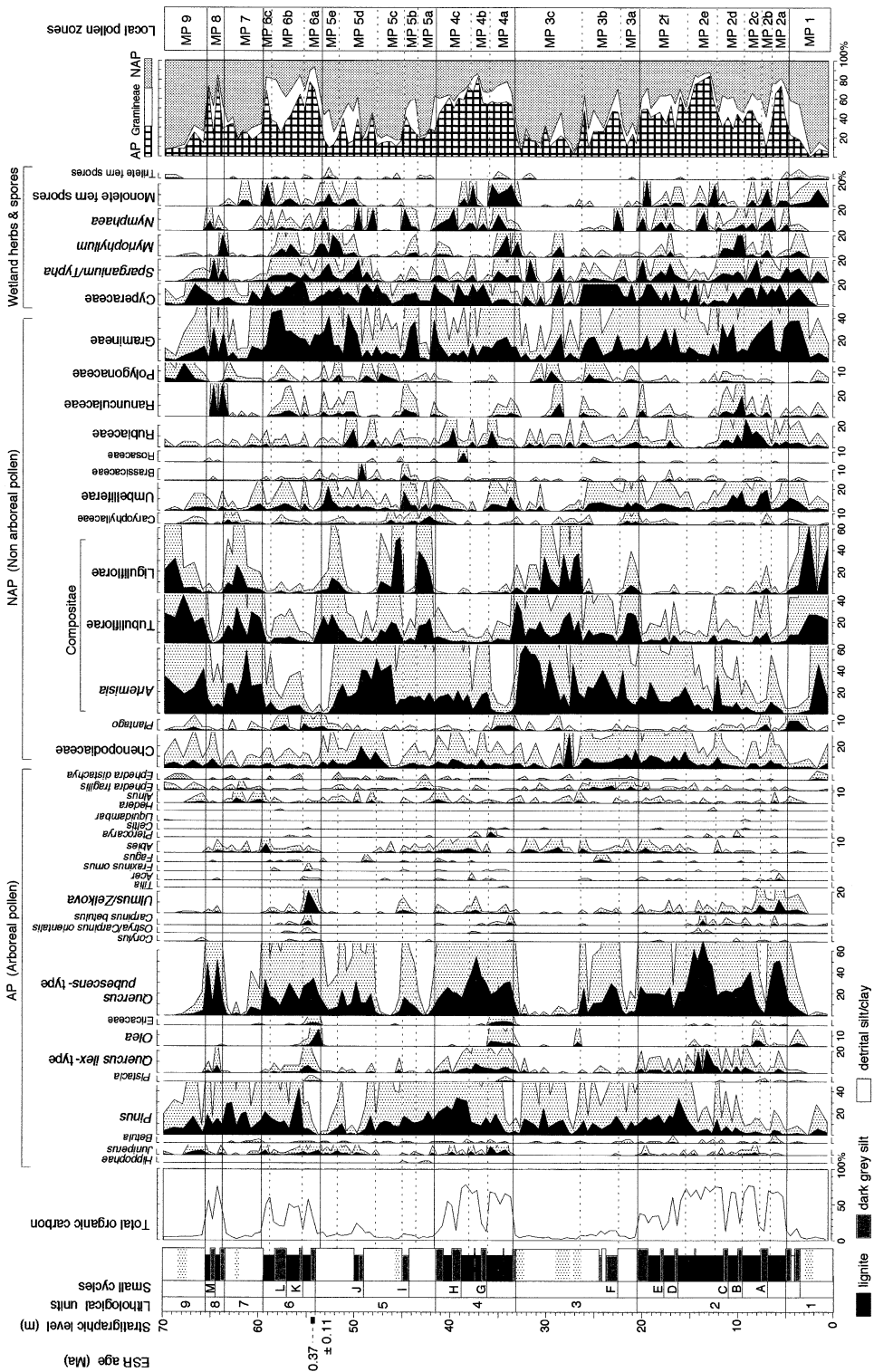


Table 2

Phase relations between the studied section and the parallel Marathousas and Choremiou sections [16] of the Middle Pleistocene Marathousa Member, Megalopolis, SW Greece

Studied section			Marathousas and Choremiou sections	
Lithological unit	Small cycle	Local pollen zone	Lignite seam	Small cycle
Unit 9		MP 9		
Unit 8*		MP 8	Lignite V	
Unit 7		MP 7		
Unit 6*		MP 6	Lignite IV	
Unit 5	layer I, J	MP 5		layer h, j
Unit 4*		MP 4	Lignite III	
Unit 3	layer F	MP 3		layer g
Unit 2*		MP 2	Lignite II	
Unit 1		MP 1	Lignite I	

Asterisks indicate lignitic units alternating with detrital units.

carbonate concretion probably of a biogenic origin exists at 37.5 m.

Unit 5 (41.5–54.0 m). Light gray to greenish-gray silt/clay. Sediment materials are generally fine with few sand grains. Organic/lignitic beds are interbedded at 44–45 m and 49–50 m, labelled I and J, respectively.

Unit 6 (54.0–59.5 m). Blackish lignite with dark gray silt/clay bands labelled K and L. Near the base of the unit, sediments are lighter in color containing abundant bivalve shells.

Unit 7 (59.5–63.5 m). Greenish-gray silt/clay. Very fine-grained sands are contained at 62–63 m.

Unit 8 (63.5–65.5 m). Blackish lignite with a dark gray silt band labelled M. The lignite contains abundant organic fractions.

Unit 9 (65.5–70.0 m). Greenish gray silt/clay. Sediment materials are coarser around 68 m.

From a test paleomagnetic analysis, we know that the sampled section is normally magnetized throughout the sequence. This means that the section is time-equivalent to the upper parts of the Marathousas and Choremiou sections, which are the parallel sections described in the northern part of the basin [16]. Phase relations between the sections are summarized in Table 2. The lignitic units

2, 4, 6 and 8 correspond to Lignites II, III, IV and V, respectively. The subordinate layers in unit 5 (layers I and J) are the counterparts of layers h and j in the Marathousas and Choremiou sections. Layer F in unit 3 corresponds to layer g. The overall lithological cycle patterns show good agreements between the sections.

Sediment samples for pollen analysis and loss-on-ignition analysis were collected in 1994 by abseiling from the top of the outcrops. The studied section consisted of staircase-like outcrops ca. 25 m high, easily integrated into a composite section based on flat, distinct bedding planes. Approximately 10 g of sediments were collected from the lignite every 50 cm. The sample size in the detrital units was ~50 g. For ESR age determination, fossil bivalve shells were collected near the bottom of unit 6 (54 m in the stratigraphic level). Surface sediments approximately 30 cm in thickness were removed to reach fresh materials. Matrix sediments around the shells were also collected and sealed carefully to prevent any moisture loss. The ESR samples were transported without being subjected to artificial X-ray radiation at airports, and were analyzed at the Department of Earth and Space Science, Osaka Univer-

←

Fig. 3. Results of pollen analysis for the Middle Pleistocene Marathousa Member, Megalopolis, SW Greece. Dotted pattern shows a five-fold magnification. In the lithological column, black indented beds represent lignite whereas white protruding beds represent detrital clay/silt. Shaded beds represent dark gray organic layers. Dotted beds contain very fine-grained sands.

sity, Japan. The palynological samples were analyzed in the pollen laboratory at the International Research Centre for Japanese Studies, Kyoto, Japan.

For the pollen analysis, sediment samples were milled and bathed in 10% HCl solution overnight to remove any calcium carbonate. After excess HCl was rinsed off, the samples were boiled in 10% KOH solution for 10 min to remove humic acids. The resulting suspension was cleaned by repeated centrifugation and decanting to remove clay-sized particles. Fossil pollen was extracted from heavier particles by heavy liquid flotation using  $ZnCl_2$  solution. Finally, the samples were acetolysed and mounted in glycerol solution. More than 300 pollen grains from trees and herbs excluding aquatics were counted for each sample and used for pollen sums for percentage calculations. Percentages of wetland pollen and spores were calculated based on a separate total pollen sum.

The procedure for loss-on-ignition analysis followed the method given in Dean [25]. Approximately 0.3 g of dry sediments were ignited at 550°C in a muffle furnace overnight, and the resulting weight losses were measured gravimetrically to determine total organic carbon (TOC). Additional ignition at higher temperature to measure carbonate carbon was omitted, because HCl treatment did not generate observable reactions indicating the presence of significant quantities of carbonate.

Pretreatment for ESR dating followed the method of Ikeya [26]. After moderate ultrasonic cleaning, shell samples were etched in 10% HCl solution for 1 min to remove surface layers with high  $\gamma$ -ray influence. The etched shells were milled into grain sizes of 100–250  $\mu m$ . Approximately 1 g of final  $CaCO_3$  powder was obtained. The initial ESR signal intensity was measured using an X-band spectrometer at Osaka University. Additive irradiation of  $\gamma$ -rays from  $^{60}Co$  source was performed up to a dose of 10 kGy, and the values of the enhanced ESR intensity were plotted on a saturation curve to calculate the total dose (TD) of the materials. The matrix sediments were used to calculate the annual dose rate (D). After being dried at 70°C for 3 days, the sediments were sub-

jected to the  $\gamma$ -ray spectroscopy to estimate concentrations of  $^{238}U$ ,  $^{232}Th$  and  $^{40}K$ . The ESR date (T) was finally determined by dividing TD by D.

## 4. Results

### 4.1. Pollen

Nine local pollen zones (MP 1–9) were established based on variations in AP/NAP (arboreal pollen/non-arboreal pollen) (Fig. 3). Even-numbered zones were dominated by tree pollen of *Quercus* and *Pinus*, whereas odd-numbered zones were dominated by Compositae herbs (*Artemisia*, Tubuliflorae and Liguliflorae). The forest phases also showed high frequencies of Gramineae, but the Gramineae were associated with abundant Cyperaceae and/or *Sparganium/Typha*, and probably derived from a reed swamp rather than from regional grasslands. An abundance of wetland grass pollen in lignite seams has consistently been observed from a marl lake in Southeast Greece [27]. Zone boundaries were placed where tree assemblages were replaced by herbaceous assemblages and vice versa. The resulting zonation was in agreement with lithological changes. Pollen preservation is generally good in the lignite seams, whereas eroded grains occur in the detrital units. Frequent fluctuations were observed among *Artemisia*, Tubuliflorae and Liguliflorae, but these were not used for further subzonation because the ecological significance of the variations remains uncertain.

#### 4.1.1. Zone MP 1 (0–5.0 m)

Zone MP 1 is dominated by Compositae. Tree taxa, excluding *Pinus*, are absent in the lower part, whereas *Q. pubescens*-type, *Q. ilex*-type, *Ulmus/Zelkova* and *Olea* increase in the upper part.

#### 4.1.2. Zone MP 2 (5.0–20.5 m)

Zone MP 2 shows high AP values (40–80%), subdivided into MP 2a–2f. Subzones MP 2a, 2c and 2e correspond to typical lignite subunits, dominated by *Q. pubescens*-type associated with *Q. ilex*-type, *Ulmus/Zelkova*, *Carpinus betulus*, *Olea*, Ericaceae, etc. By contrast, subzones MP

2b, 2d and 2f correspond to layers A, B–C and D–E in lithology, yielding more abundant *Pinus*, *Abies*, Chenopodiaceae, *Artemisia* and/or Tubuliflorae. Subzone MP 2e is marked by the highest values of *Quercus* (*pubescens*- and *ilex*-types) in the sequence. Subzone MP 2f shows regularly moderate frequencies of *Pinus*, *Abies* and *Artemisia*.

#### 4.1.3. Zone MP 3 (20.5–33.5 m)

Zone MP 3 is dominated by Compositae, but the AP increase into 30–40% in and around layer F. *Quercus pubescens*-type is abundant in 22–26 m (i.e., MP 3b). In subzone MP 3c, *Pinus* and *Abies* persist but temperate trees almost disappear.

#### 4.1.4. Zone MP 4 (33.5–41.5 m)

Zone MP 4 shows high AP values (50–80%). Subzone MP 4a is dominated by *Q. pubescens*-type, associated with *Q. ilex*-type, *Olea*, Ericaceae, *C. betulus*, *Ulmus/Zelkova*, etc. No *Artemisia* but Gramineae are abundant. The end of this diversified palynoflora is signified by the deposition of layer G where *Artemisia* increases to moderate values. Subzone MP 4b differs from MP 4a by the absence of *Olea* and Ericaceae as well as a prominent peak of *Q. pubescens*-type. *Artemisia* shows an increase in the beginning of this subzone. Subzone MP 4c shows abundant *Pinus* with higher but moderate frequencies of *Abies* and *Artemisia*.

#### 4.1.5. Zone MP 5 (41.5–53.5 m)

Zone MP 5 is dominated by Compositae especially in subzones MP 5a, 5c and 5e. Subzones MP 5b and 5d, containing layers I and J in lithology, show increases in *Q. pubescens*-type whereas *Quercus* is almost absent in subzones 5a and 5c. *Pinus* and *Abies* are persistent during subzones MP 5a–c. *Artemisia* shows very high values in subzone MP 5c.

#### 4.1.6. Zone MP 6 (53.5–59.5 m)

Zone MP 6 shows high AP values (30–80%). Subzone MP 6a provides the lowest value of NAP minus Gramineae in the record (9%). Prominent peaks of *Ulmus/Zelkova* and *Olea* are very characteristic. The top of this subzone is marked by layer K in lithology. Subzone MP 6b shows

more abundant *Pinus*, *Artemisia* and Tubuliflorae. A decline of AP is observed in layer L. Subzone MP 6c is recognized by returns to a short but significant forest phase. *Abies* yields the maximum value (8%) in the record.

#### 4.1.7. Zone MP 7 (59.5–63.75 m)

Zone MP 7 is dominated by Compositae. Temperate trees are rare whereas *Pinus* and *Abies* are persistent during MP 7.

#### 4.1.8. Zone MP 8 (63.75–65.5 m)

Zone MP 8 is dominated by *Q. pubescens*-type with very low values of *Artemisia*. Layer M yields a single spectrum with lower AP. *Pinus* and *Abies* appear to persist during the zone.

#### 4.1.9. Zone MP 9 (65.5–70.0 m)

Zone MP 9 is dominated by Compositae. Tree taxa other than *Pinus* are completely absent in the upper part of the zone.

### 4.2. Loss on ignition

Results from loss-on-ignition analysis indicate that the lithological changes seen in the studied section are geochemically expressed as variations in TOC. Zones MP 1, 3, 5, 7 and 9 are characterized by low TOC, while zones MP 2, 4, 6 and 8 show generally high TOC. In the blackish lignite, the TOC shows high values (50–70%), whereas the light-colored detrital muds contain little organic carbon (<5%). The uppermost lignite in unit 2 exceptionally shows lower carbon contents (30–40%) than other typical lignites. The ignition loss result also indicates a moderately organic composition in the subordinate layers, with the TOC of 10–30%.

### 4.3. ESR dating

The ESR date (T) for shell samples from the base of unit 6 (54 m in the stratigraphic level) was determined as  $0.37 \pm 0.11$  Ma ( $2\sigma$ ). The total dose (TD) and annual dose rate (D) were calculated as  $170 \pm 50$  Gy and  $0.47 \pm 0.01$  mGy/yr, respectively. Average concentrations of  $^{238}\text{U}$ ,  $^{232}\text{Th}$  and  $^{40}\text{K}$  in the matrix sediments, on which the annual dose

rate is based, were  $2.3 \pm 0.1$  ppm,  $8.2 \pm 0.2$  ppm and  $1.9 \pm 0.0\%$ , respectively.

## 5. Discussion

### 5.1. Vegetation and climate

The palynological results yield a continuous profile of vegetation and paleoclimate throughout the Marathousa Member. The lignitic units 2, 4 and 6 (Lignites II, III and IV) are characterized by temperate forest of *Quercus* (oak) associated with *Ulmus/Zelkova*, *Acer*, *Carpinus*, etc. This assemblage is consistent with the interglacial palynoflora of southern Europe [27–29]. Mediterranean evergreen trees (*Q. ilex*-type, *Olea* and Ericaceae) occur in the lower parts of the lignite seams, as the consequence of full vegetation development in the early forest phases. Temperate deciduous trees increase subsequently, followed by conifer trees in the upper parts. This vegetation succession is reminiscent of the ‘interglacial vegetation succession’, representing sequential tree expansion in Late Pleistocene interglacial episodes [30]. The warm climate with reduced effective moisture in the early interglacial periods allows the growth of Mediterranean evergreen trees. The oak-dominated palynoflora in the lignite seams are consistent with the previous pollen data from basal Lignite I [20]. By contrast, detrital units 1, 3, 5, 7 and 9 represent cold *Artemisia* steppe. Abundant Tubuliflorae and Liguliflorae occur, and this flora is generally common to the last glacial flora in the Eastern Mediterranean [27,31]. All these vegetation reconstructions are coherent, providing interglacial origins for the lignite seams and glacial origins for the detrital beds.

The attribution of a complete lignite-detritus couplet to a glacial/interglacial cycle gives units 1–6 a time coverage of approximately 300 kyr. The ESR dating yields a radiometric age of  $0.37 \pm 0.11$  Ma for the basal part of unit 6. Using 0.78 Ma as the age of the Brunhes/Matuyama paleomagnetic boundary [32,33], which lies below unit 1 at Megalopolis [16], the time interval of units 1–6 falls within the range of 300–520 kyr. These two estimated time ranges are in agreement.

One of us [16] has suggested a reasonable average sedimentation rate (21 cm/kyr) for the Marathousa Member by giving the 100-kyr periodicity to the lignite–detritus alternation also.

### 5.2. Astronomical cycles

The reconstructed paleoclimate history points out the astronomical forcing on the lithological cycles at Megalopolis. The first-order cycle is obviously attributed to the 100-kyr component of the orbital eccentricity cycle [34,35]. Here we indicate that the second-order lithological cycle of the Marathousa Member is also astronomically induced. In many cases, recognition of orbital forcing on sedimentary cycles is accomplished by first demonstrating a climatic origin for the cycle and subsequently finding an average duration that is consistent with one of the known Milankovitch periods. In this study, the palynological results detect meaningful climate changes in and around the labelled layers. Subordinate organic layers in the detrital units (layers F, I and J) show increases in *Quercus* at the expense of *Artemisia*, representing temporal expansion of open oak forests within steppes. The second-order cycle appears somewhat intricate in the lignite seams, but many of them do provide meaningful changes in the pollen record. The lower *Quercus* values around layers G, H, etc reflect temporal deforestation. Two labelled layers B and E, with no independent palynological changes, are here included into composite layers B–C and D–E. We note that the subordinate organic layers generally show intermediate features between the lignites and detrital muds both in the pollen and TOC records. These are logically the result of intermediate climate conditions between full glacials and interglacials (i.e., interstadials in glacial periods and temporal coolings in interglacial periods). Therefore, smaller-scale climate fluctuations are recognized in and around layers A, B–C, D–E and F in units 2–3, and layers G, H, I and J in units 4–5. The unlabelled layers at unit boundaries are not considered because they probably represent transitional zones between glacials and interglacials instead of independent climate events. The total number of climatic subunits in a complete lignite–detritus cou-

plet is thus five, giving an approximately 20-kyr periodicity for the climate fluctuations. This is in agreement with the 21-kyr insolation (precession) cycle, which was deduced from the 65°N summer insolation [34] and is now recognized as a reliable external target curve [36]. We suggest that the second-order lithological cycle in the Marathousa Member is regulated by the insolation cycle. This is currently based on a rough calculation, but it provides a likely scenario when comparable case studies from the Ptolemais basin, northern Greece [19] and the Lupoia basin, southern Romania [37] are considered.

There is another comparable palynological dataset obtained from Tenaghi Philippon (Drama), NE Greece [38]. This was based on frequency analyses applied to time series of different vegetation types transformed from the past 975 000-yr pollen record [28,29,31]. Using the moving window technique, periods of 95–99 ka, 40–44 ka and 19–21 ka, related to the orbital forcing, were recognized in the lower Middle Pleistocene. In particular, the 19–21-ka cycle seen in the variation curves of local vegetation types implies an influence of the precession cycle on hydrological balance in the Drama basin. This supports our

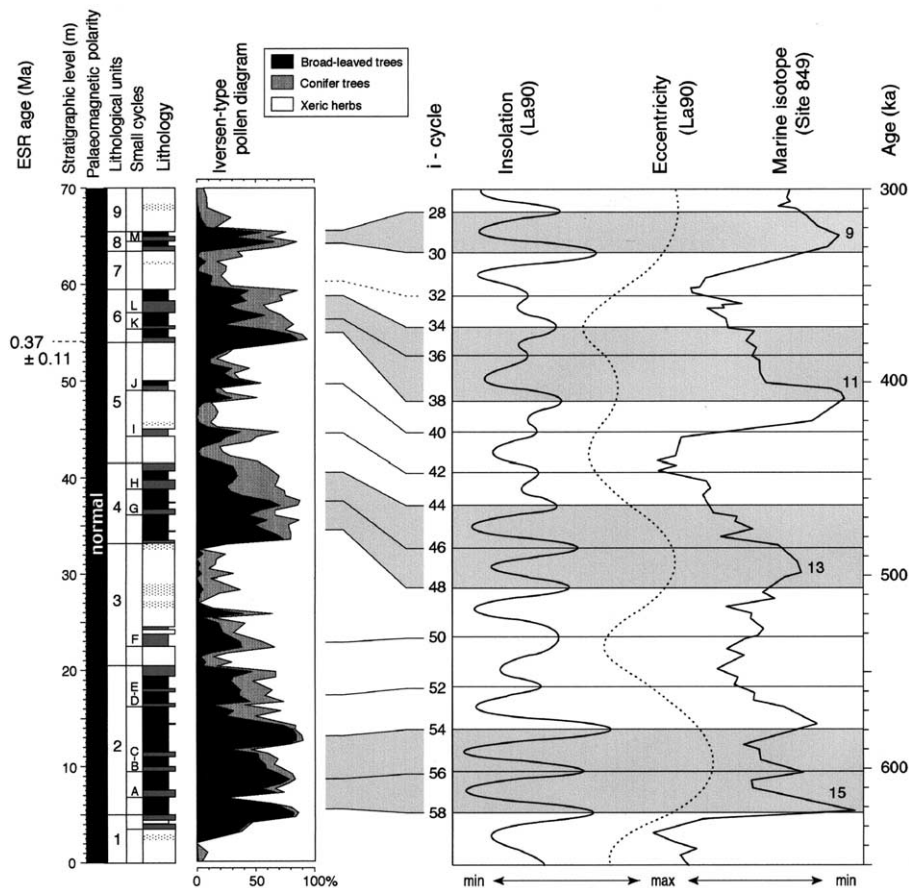


Fig. 4. Tentative correlation between the lithological cycles in the studied section, astronomical cycles [34] and marine oxygen isotope stratigraphy [40,41]. Intercorrelation between the external target curves is after van Vugt et al. [16]. The i-cycle codification of insolation peaks is based on Lourens et al. [36]. In the Iversen-type pollen diagram, 'xeric herbs' contain Compositae (*Artemisia*, *Tubuliflorae* and *Liguliflorae*), *Chenopodiaceae*, *Plantago* and *Caryophyllaceae*. 'Conifer trees' contain *Pinus*, *Abies*, *Juniperus* and *Ephedra*. In the lithological column, layers B and E with no meaningful palynological changes are included in composite layers B–C and D–E.

arguments in the time-equivalent Megalopolis basin. There is no strong evidence to address the presence or absence of the 41-kyr obliquity cycle at Megalopolis.

### 5.3. Tentative time frame

Recognition of astronomical cycles in a geological record can allow astronomical calibration techniques [9,39] based on ‘tuning’ of sedimentary cycle patterns to variations in the Earth’s orbital parameters. Unfortunately, the lack of sufficient time control prevents the unambiguous tuning for the studied section. Here we suggest a tentative phase relation between the lithological cycles and external target curves [34,40,41] (Fig. 4). This is based on assumptions that unit 6 correlates with marine isotope stage (MIS) 11 and that no major hiatuses occur throughout the sequence. The ESR date of  $0.37 \pm 0.11$  Ma ( $2\sigma$ ) at the base of unit 6 points to MIS 9 (ca. 330 ka) or MIS 11 (ca. 420 ka) as likely marine counterparts for the unit. Of these two candidates, MIS 11 is palynologically preferred because of the unique unit 6 palynoflora with abundant *Ulmus/Zelkova*. In the Ioannina basin, NW Greece, a prominent peak of *Ulmus/Zelkova* was reported from the MIS 11 phase [42]. We also note that unit 6 is marked by the higher frequencies of *Olea*. The warmer MIS 11 interglacial [43,44] may have allowed an expansion of elm on wetter mountain flanks (mid elevation) of western Greece (including Ioannina and Megalopolis) and a simultaneous spread of olives in drier southern Greece (including Megalopolis), at the beginning of MIS 11. As to the continuity of the section, it is possible that small hiatuses occur at the unit boundaries. However, large hiatuses (containing one or more glacial cycles) are unlikely to exist because the studied section nowhere extends back to the Brunhes/Matuyama paleomagnetic boundary (i.e., MIS 19). The timescale proposed in Fig. 4 provides counterparts for the insolation peaks 28–58 [36].

A reasonable time–depth relationship with an almost linear sedimentation curve and an average sedimentation rate of 0.2 mm/yr is deduced from Fig. 4 (Fig. 5). A decline in the uppermost part of

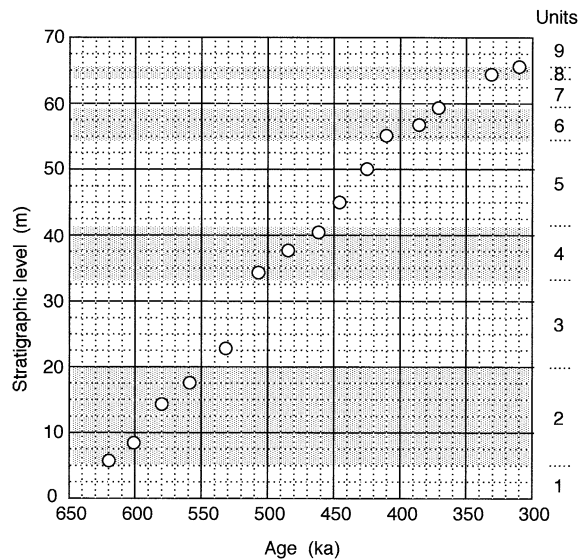


Fig. 5. A provisional time–depth relationship for the studied section of the Marathousa Member, Megalopolis, SW Greece. Note that this curve is based on a tentative time frame in Fig. 4.

the accumulation curve suggests decelerated aggradation near the termination of lacustrine environments. This is consistent with fluvial deposits of the Megalopolis Formation which stratigraphically overlie the Marathousa Member [22] (Table 1). Our timescale can also give a coherent chronostratigraphy for the late Pleistocene deposits above the Megalopolis Formation. It is feasible that the Thoknia and Potamia formations, a pair comprising brown loams and fluvial sands/gravels (Table 1), represent the last glacial cycle (stages 5–2) and the penultimate glacial cycle (stages 7–6), respectively.

Nevertheless, the original aim of Fig. 4 is to confirm the influence of astronomical forcing on the Megalopolis basin, and we emphasize that the proposed time frame is tentative. The correlation is not robust yet and some alternatives can exist under the current time control. For example, unit 3 with a highly herbaceous flora could be an equivalent of the extensive MIS 12 glacial [29]. This could create an optional chronology correlating units 2, 4 and 6 with MIS 13, 11 and 9, respectively. This does not explain the unique unit 6 palynoflora but is consistent with the ESR age. One of us [16] has suggested another alternative

that correlates Lignites II, III, IV and V (i.e., units 2, 4, 6 and 8) with MIS 17, 15, 13 and 11, respectively, based on paleomagnetic and cyclostratigraphic results from the parallel Marathoussas and Choremiou sections. This option is, at present, less consistent with the pollen and the ESR results, however.

#### 5.4. Local environments and hydrological balance

We feel it necessary to address sedimentary environments and moisture balance in the Megalopolis basin. Both lithological and palynological features, which show lignites with emergent aquatic herbs such as Cyperaceae and Gramineae (probably *Phragmites*), provide local swamp vegetation for the interglacial periods. The subordinate layers consisting of gyttja-like organic muds with molluscan shells indicate increased lake levels. By contrast, the glacial deposits yield little biological evidence. As to lithological features, the inorganic muds with few coarse materials imply lacustrine environments with high water tables. This appears to be inconsistent with a few recent lake level studies in Greece reporting lowered lake levels at the Last Glacial Maximum (LGM) (e.g., [45]). Nevertheless, our implication is consistent with regionally synchronous high LGM lake levels in the northern Mediterranean to the Middle East [46,47]. Reduced evapotranspiration resulting from low temperature and/or increased cloudiness during full glacials [48] allows the coincidence of increased runoff into the lake and reduced soil moisture [49,50]. This explains the high lake levels and simultaneous semi-arid steppes at Megalopolis. The dark gray layers were formed under intermediate local environments between the lakes and swamps. Abundant *Nymphaea* in layers F, I and J suggests water depths < 3–5 m [46].

There is no evidence giving a fluvial origin for the glacial deposits. The detrital muds are massive with generally fine grain sizes. Nevertheless, several bands of very fine-grained sands are associated with abundant Liguliflorae pollen that is not common in the glacial palynoflora of Greece. This may indicate strengthened river influences. Otherwise, it may be the result of differential preserva-

tion of pollen grains. The detrital muds have significantly lower pollen concentrations with poorer pollen preservation. Although such features are common for glacial deposits in the Mediterranean (e.g., [42]), these put a certain restraint on strict interpretations for glacial environments based on a single palynological dataset.

## 6. Conclusions

This paper aims to demonstrate the astronomical origins of lithological cycles in the lignite-bearing Marathoussa Member, Megalopolis, SW Greece. Palynological evidence reveals the climate origins of the thick lignite seams and thin organic layers, attributing the different lithological cycles to the 100-kyr eccentricity cycle and the 21-kyr insolation cycle, respectively. Paleoenvironments and sedimentation in this small continental basin are regulated by the Earth's orbital forcing through variations in temperature and hydrological balance. There is no strong evidence to address the obliquity cycle at Megalopolis. A tentative phase relation with external target curves is shown to demonstrate the probability of astronomical forcing on the Megalopolis basin. All counterparts of insolation peaks 28–58 [43] can be seen in the lithological cycle, giving a provisional time coverage of ca. 300–650 kyr to the studied section.

## Acknowledgements

Prof. Dr. F. Masuda of Kyoto University spared his time to read our manuscript and gave useful suggestions. Dr. H. Kohno and Dr. A. Tani of Osaka University gave technical guidance concerning ESR dating. We appreciate the helpful comments received during journal review from Dr. P.C. Tzedakis, Dr. D. Magri and an anonymous reviewer. We are grateful to Dr. Y. Brousoulis of the Institute of Geology and Mineral Exploration, Athens and the employees of the coal mines at Megalopolis for their enormous help during our field work. This work was supported by the Yangtze River Civilization Pro-

gramme (YRCP) of the International Research Centre for Japanese Studies and the Research Promotion Fund of Doshisha University, Kyoto, Japan. [BARD]

## References

- [1] L. Tauxe, N.D. Opdyke, G. Pasini, C. Elmi, Age of the Plio–Pleistocene boundary in the Vrica section, southern Italy, *Nature* 304 (1983) 125–129.
- [2] J.D.A. Zijderveld, F.J. Hilgen, C.G. Langereis, P.J.J.M. Verhallen, W.J. Zachariasse, Integrated magnetostratigraphy and biostratigraphy of the Upper Pliocene–Lower Pleistocene from the Monte Singa and Crotone areas in Calabria, Italy, *Earth Planet. Sci. Lett.* 107 (1991) 697–714.
- [3] C.G. Langereis, F.J. Hilgen, The Rossello composite: a Mediterranean and global reference section for the Early to early Late Pliocene, *Earth Planet. Sci. Lett.* 104 (1991) 211–225.
- [4] W. Krijgsman, C.G. Langereis, R. Daams, A.J. van der Meulen, Magnetostratigraphic dating of the middle Miocene climate change in the continental deposits of the Aragonian type area in the Calatayud–Teruel basin (Central Spain), *Earth Planet. Sci. Lett.* 128 (1994) 513–526.
- [5] F.J. Hilgen, L. Bissoli, S. Iaccarino, W. Krijgsman, R. Meijer, A. Negri, G. Villa, Integrated stratigraphy and astrochronology of the Messinian GSSP at Oued Akrech (Atlantic Morocco), *Earth Planet. Sci. Lett.* 182 (2000) 237–251.
- [6] J.D. Hays, J. Imbrie, N.J. Shackleton, Variations in the Earth's orbit: pacemaker of the ice ages, *Science* 194 (1976) 1121–1132.
- [7] J. Imbrie, J.D. Hays, D.G. Martinson, A. McIntyre, A.C. Mix, J.J. Morley, N.G. Pisias, W.L. Prell, N.J. Shackleton, The orbital theory of Pleistocene climate: support for a revised chronology of the marine oxygen isotope record, in: A. Berger, J. Imbrie, J. Hays, G. Kukla, B. Saltzman (Eds.), *Milankovitch and Climate, Part 1*, Reidel, Dordrecht, 1984, pp. 269–305.
- [8] M. Rossignol-Strick, African monsoons, an immediate climate response to orbital insolation, *Nature* 304 (1983) 46–49.
- [9] F.J. Hilgen, Astronomical calibration of Gauss to Matuyama sapropels in the Mediterranean and implication for the geomagnetic polarity timescale, *Earth Planet. Sci. Lett.* 104 (1991) 226–244.
- [10] F.J. Hilgen, Extension of the astronomically calibrated (polarity) timescale to the Miocene–Pliocene boundary, *Earth Planet. Sci. Lett.* 107 (1991) 349–368.
- [11] N.J. Shackleton, S. Crowhurst, T. Hagelberg, N.G. Pisias, D.A. Schneider, A new Late Neogene time scale: application to Leg 138 sites, *Proc. ODP Sci. Results* 138 (1995) 73–97.
- [12] F.J. Hilgen, W. Krijgsman, C.G. Langereis, L.J. Lourens, A. Santarelli, W.J. Zachariasse, Extending the astronomical (polarity) time scale into the Miocene, *Earth Planet. Sci. Lett.* 136 (1995) 495–510.
- [13] W. Krijgsman, W. Delahaije, C.G. Langereis, P.L. de Boer, Cyclicity and NRM acquisition in the Armantes section (Miocene, Spain): potential for an astronomical polarity time scale for the continental record, *Geophys. Res. Lett.* 24 (1997) 1027–1030.
- [14] J. Steenbrink, N. van Vugt, F.J. Hilgen, J.R. Wijbrans, J.E. Meulenkamp, Sedimentary cycles and volcanic ash beds in the Lower Pliocene lacustrine succession of Ptolemais (NW Greece): discrepancy between  $^{40}\text{Ar}/^{39}\text{Ar}$  and astronomical ages, *Palaeogeogr. Palaeoclimatol. Palaeoecol.* 152 (1999) 283–303.
- [15] H. Abdul Aziz, F.J. Hilgen, W. Krijgsman, E. Sanz-Rubio, J.P. Calvo, Orbital forcing of sedimentary cycles in the Miocene continental Calatayud Basin (NE Spain), *Earth Planet. Sci. Lett.* 177 (2000) 9–22.
- [16] N. van Vugt, H. de Bruijn, M. van Kolfshoten, C.G. Langereis, Magneto- and cyclostratigraphy and mammal-faunas of the Pleistocene lacustrine Megalopolis Basin, Peloponnesos, Greece, *Geol. Ultraiectina* 189 (2000) 69–92.
- [17] F.J. Hilgen, H. Abdul Aziz, W. Krijgsman, C.G. Langereis, L.J. Lourens, J.E. Meulenkamp, I. Raffi, J. Steenbrink, E. Turco, N. van Vugt, J.R. Wijbrans, W.J. Zachariasse, Present status of the astronomical (polarity) time-scale for the Mediterranean Late Neogene, *Phil. Trans. R. Soc. London A* 357 (1999) 1931–1947.
- [18] W. Krijgsman, F.J. Hilgen, I. Raffi, F.J. Sierro, D.S. Wilson, Chronology, causes and progression of the Messinian salinity crisis, *Nature* 400 (1999) 652–655.
- [19] N. van Vugt, J. Steenbrink, C.G. Langereis, F.J. Hilgen, J.E. Meulenkamp, Magnetostratigraphy-based astronomical tuning of the early Pliocene lacustrine sediments of Ptolemais (NW Greece) and bed-to-bed correlation with the marine record, *Earth Planet. Sci. Lett.* 164 (1998) 535–551.
- [20] B. Nickel, W. Riegel, T. Schönherr, E. Velitzelos, Environments of coal formation in the Pleistocene lignite at Megalopolis, Peloponnesus (Greece) – reconstructions from palynological and petrological investigations, *N. Jahrb. Geol. Paläontol. Abh.* 200 (1996) 201–220.
- [21] G. Lüttig, G. Marinos, Zur Geologie der neuen griechischen Braunkohlen-Lagerstätte von Megalopolis, *Braunkohle* 6 (1962) 222–231.
- [22] R. von Vinken, Stratigraphie und Tektonik des Beckens von Megalopolis (Peloponnes, Griechenland), *Geol. Jahrb.* 83 (1965) 97–148.
- [23] H. Hiltermann, G. Lüttig, Biofazies und Paleolimnologie der Pliozänen und Pleistozänen Seen im Megalopolis-Becken (Peloponnes), *Mitt. Int. Ver. Limnol.* 17 (1969) 306–314.
- [24] O. Polunin, *Flowers of Greece and the Balkans – a Field Guide*, Oxford University Press, Oxford, 1980, 389 pp.
- [25] W.E. Dean Jr., Determination of carbonate and organic matter in calcareous sediments and sedimentary rocks by

- loss on ignition: comparison with other methods, *J. Sediment. Petrol.* 44 (1974) 242–248.
- [26] M. Ikeya, *New Applications of Electron Spin Resonance*, World Scientific, Singapore, 1993, 317 pp.
- [27] M. Okuda, Y. Yasuda, T. Setoguchi, Middle to Late Pleistocene vegetation history and climatic changes at Lake Kopais, Southeast Greece, *Boreas* 30 (2001) 73–82.
- [28] T.A. Wijmstra, A. Smit, Palynology of the middle part (30–78 metres) of the 120 m deep section in Northern Greece (Macedonia), *Acta Bot. Neerl.* 25 (1976) 297–312.
- [29] A.M. van der Wiel, T.A. Wijmstra, Palynology of the lower part (78–120 m) of the core Tenaghi Philippon II, Middle Pleistocene of Macedonia, Greece, *Rev. Palaeobot. Palynol.* 52 (1987) 73–88.
- [30] P.C. Tzedakis, K.D. Bennett, Interglacial vegetation succession: a view from southern Europe, *Quat. Sci. Rev.* 14 (1995) 967–982.
- [31] T.A. Wijmstra, Palynology of the first 30 metres of a 120 m deep section in Northern Greece, *Acta Bot. Neerl.* 18 (1969) 511–527.
- [32] L. Tauxe, A.D. Deino, A.K. Behrensmeier, R. Potts, Pinning down the Brunhes/Matuyama and upper Jaramillo boundaries: a reconciliation of orbital and isotopic time scales, *Earth Planet. Sci. Lett.* 109 (1992) 561–572.
- [33] F.C. Bassinot, L.D. Labeyrie, E. Vincent, X. Quidelleur, N.J. Shackleton, Y. Lancelot, The astronomical theory of climate and the age of the Brunhes–Matuyama magnetic reversal, *Earth Planet. Sci. Lett.* 126 (1994) 91–108.
- [34] J. Laskar, The chaotic motion of the solar system: a numerical estimate of the size of the chaotic zones, *Icarus* 88 (1990) 266–291.
- [35] A. Berger, M.F. Loutre, Insolation values for the climate of the past 10 m.y., *Quat. Sci. Rev.* 10 (1991) 297–317.
- [36] L.J. Lourens, A. Antonarakou, F.J. Hilgen, A.A.M. van Hoof, C. Vergnaud-Grazzini, W.J. Zachariasse, Evaluation of the Plio–Pleistocene astronomical timescale, *Paleoceanography* 11 (1996) 391–413.
- [37] N. van Vugt, C.G. Langereis, F.J. Hilgen, Dominant expression of eccentricity versus precession in the lithology of Mediterranean continental (lacustrine) deposits, *Geol. Ultraiectina* 189 (2000) 93–108.
- [38] H.J.P.M. Mommersteeg, M.F. Loutre, R. Young, T.A. Wijmstra, H. Hooghiemstra, Orbital forced frequencies in the 975 000 year pollen record from Tenaghi Philippon (Greece), *Clim. Dyn.* 11 (1995) 4–24.
- [39] N.J. Shackleton, A. Berger, W.R. Peltier, An alternative astronomical calibration of the lower Pleistocene time scale based on ODP site 677, *Trans. R. Soc. Edinburgh Earth Sci.* 81 (1990) 251–261.
- [40] A.C. Mix, J. Le, N.J. Shackleton, Benthic foraminiferal stable isotope stratigraphy of Site 846: 0–1.8 Ma, *Proc. ODP Sci. Results* 138 (1995) 839–854.
- [41] M.E. Raymo, The timing of major climate terminations, *Paleoceanography* 12 (1997) 577–585.
- [42] P.C. Tzedakis, Vegetation change through glacial-interglacial cycles: a long pollen sequence perspective, *Phil. Trans. R. Soc. London B* 345 (1994) 403–432.
- [43] L.H. Burckle, Late Quaternary interglacial stages warmer than present, *Quat. Sci. Rev.* 12 (1993) 825–831.
- [44] W.R. Howard, A warm future in the past, *Nature* 388 (1997) 418–419.
- [45] G. Digerfeldt, S. Olsson, P. Sandgren, Reconstruction of lake-level changes in lake Xinias, central Greece, during the last 40 000 years, *Palaeogeogr. Palaeoclimatol. Palaeoecol.* 158 (2000) 65–82.
- [46] S.P. Harrison, G. Digerfeldt, European lakes as palaeohydrological and palaeoclimatic indicators, *Quat. Sci. Rev.* 12 (1993) 233–248.
- [47] S.P. Harrison, G. Yu, P.E. Tarasov, Late Quaternary lake-level record from northern Eurasia, *Quat. Res.* 45 (1996) 138–159.
- [48] COHMAP Members, Climatic changes of the last 18 000 years: observations and model simulations, *Science* 241 (1988) 1043–1052.
- [49] N. Roberts, Age, palaeoenvironments, and climatic significance of late Pleistocene Konya Lake, Turkey, *Quat. Res.* 19 (1983) 154–171.
- [50] C. Prentice, J. Guiot, S.P. Harrison, Mediterranean vegetation, lake levels and palaeoclimate at the Last Glacial Maximum, *Nature* 360 (1992) 658–660.